

Where is the Inner Edge of an Accretion Disk Around a Black Hole?

Julian H. Krolik

Physics and Astronomy Department, Johns Hopkins University, Baltimore, MD 21218

John F. Hawley

Department of Astronomy, University of Virginia, Charlottesville VA 22903

ABSTRACT

What is meant by the “inner edge” of an accretion disk around a black hole depends on the property that defines the edge. We discuss four such definitions using data from recent high-resolution numerical simulations. These are: the “turbulence edge”, where flux-freezing becomes more important than turbulence in determining the magnetic field structure; the “stress edge”, where plunging matter loses dynamical contact with the outer accretion flow; the “reflection edge”, the smallest radius capable of producing significant X-ray reflection features; and the “radiation edge”, the innermost place from which significant luminosity emerges. All these edges are dependent on the accretion rate and are non-axisymmetric and time-variable. Although all are generally located in the vicinity of the marginally stable orbit, significant displacements can occur, and data interpretations placing the disk edge precisely at this point can be misleading. If observations are to be used successfully as diagnostics of accretion in strong gravity, the models used to interpret them must take careful account of these distinctions.

Subject headings: accretion, accretion disks, instabilities, MHD, black hole physics

1. Introduction

Accretion disks around a star end at the star’s surface; the inner radius of a disk around a black hole is less well determined. Because black holes have no hard surface, more complicated dynamical processes define what is meant by a disk’s “inner edge.” The best-known of these arises from general relativity itself, which forbids stable circular orbits inside the critical radius of the marginally stable orbit, r_{ms} , not far outside the event horizon.

In a standard thin accretion disk, gas follows very nearly circular orbits and drifts inward because a nonzero stress removes angular momentum from fluid elements and transfers it outward. Inside r_{ms} , fluid elements can spiral into the hole on free-fall orbits, i.e., without further loss of angular momentum or energy. In many treatments of black hole accretion disks, it is therefore explicitly (or tacitly) assumed that the inner edge of the disk is at, or at least very close to, r_{ms} .

Although there is clearly a dynamical transition from rotational support to free-fall that must occur in the vicinity of r_{ms} , whether this constitutes the disk inner boundary depends on precisely what one means by that term. The location of the inner edge relative to r_{ms} depends on which property one is examining, and departures from r_{ms} can, in many instances, be significant. Dynamical issues require a different definition from observational characteristics.

For example, one definition of inner boundary is the innermost radius from which significant luminosity emerges to the outside world, the *radiation edge*. The inner regions of disks may grow dim for a variety of reasons: a decrease in the radiative efficiency due to flow dynamics, gravitational redshift and other general relativistic effects, cessation of dissipative heating (as in Page & Thorne 1974), or photon trapping (an effect particularly strong in “slim disks”, Abramowicz et al. 1988). All of these effects taken together determine precisely where the disk ceases to radiate.

As another example, even if little radiation originates from gas near the hole, there may still be enough material inside r_{ms} to reflect and reprocess incident X-ray photons. Reynolds & Begelman (1997) suggested that this effect may explain the shape of the Fe $K\alpha$ line in MCG–6-30-15. To what extent this is possible depends on details of the accretion flow (e.g., Young, Ross & Fabian 1998). Thus, for any particular accretion state, one may define a *reflection edge* that may be well separated from the marginally stable orbit—or from the radiation inner edge. This distinction is an important one: for example, the assumption that the reflection edge is identical to r_{ms} has been used as the basis for determining the spin parameter of a black hole (Wilms et al. 2002).

Other inner edge definitions are based not on radiative properties, but on the underlying dynamics. The *stress edge* can be defined as the point where accreting matter loses dynamical contact with the disk it left behind. In a purely hydrodynamic model using the traditional Shakura-Sunyaev α stress proportional to the pressure, this edge would be quite close to r_{ms} because of the rapid drop in pressure as the gas accelerates inward (e.g., Abramowicz & Kato 1989). Our growing confidence that magnetic stresses account for angular momentum transfer within disks (Balbus & Hawley 1998), however, has modified this view. Magnetic stress can continue well inside r_{ms} (Krolik 1999a; Gammie 1999; Hawley & Krolik 2001, 2002, hereafter HK01, HK02; Reynolds & Armitage 2001), so r_{ms} may not be a good estimate of the stress edge.

Yet another inner edge, which should generally be outside the stress edge, is the *turbulence edge*. This is the place where the magnetic field switches from being controlled by the mechanics of saturated magnetohydrodynamic (MHD) turbulence to simple flux-freezing. Here the internal disk structure begins to change, as the gas prepares for its final plunge.

Although we speak of these as edges, we emphasize that none of them is sharp. At any given instant the scale lengths of the transitions in question can be comparable to the radius. Further, because the flows are very strongly time-variable, instantaneous edge positions can change substantially from time to time. Consequently, all of them should be thought of in terms of zones within which the relevant transition can occur.

In this paper we use data from recent black hole accretion simulations for a dual purpose. On

the one hand, we examine and clarify the quantitative relations between the different inner edge definitions. Our aim is to create a conceptual framework and an associated language for discussing these issues. As our understanding of accretion dynamics deepens, we expect these distinctions to become more prominent.

On the other hand, we also develop several observational consequences of these distinctions. As we enter an era in which detailed models are fit to a variety of relativistically-shifted and broadened features, it is important to clearly define the radial emissivity distributions governing these features. Precision on these issues is vital when observations are to be used as direct tests of specific general relativistic properties of black holes. Although the numerical values we present for some of these quantities are uncertain because of the approximations made in current simulations, data from future simulations, when employed in the framework defined here, should enable finer definition of these edges and therefore more reliable inferences.

2. The Turbulence Edge

We begin with the disk edges that are defined in terms of dynamical properties. Disk dynamics are governed by MHD turbulence and the resulting Maxwell stresses. Within the disk, the intensity and structure of the magnetic field are determined by a balance between the underlying magneto-rotational instability, or MRI (Balbus & Hawley 1991), which generates the field, and the field loss terms, including local resistive dissipation of short length-scale fluctuations, and upward motion of buoyant magnetic flux (as studied, e.g., by Miller & Stone 2000). At large radius the timescales for these processes are short compared to the inflow time, but close to r_{ms} the time required for energy to travel down the turbulent cascade becomes longer than the inflow time, and the magnetic field instead evolves by flux-freezing. We define the *turbulence edge* as the boundary between the region where the magnetic field dynamics are dominated by the turbulent cascade and the region controlled by flux-freezing.

The location of this edge may be estimated in any of several ways. We can compare the timescales for the competing processes, or we can look for a change in the field structure due to this transition, or we can compare the magnitude of the turbulent velocities to the magnitude of the inflow speed. We will take up each of these in turn.

2.1. Timescales

Consider the timescale approach first. In a time-steady disk with accretion rate \dot{M} , the azimuthally- and vertically-integrated energy per unit area available for dissipation at (cylindrical) radius r is the difference between the net deposition of potential energy by accretion and the

net work done by inter-ring torques:

$$Q = \frac{-\dot{M}}{2\pi r} \frac{d}{dr} [E_B + \Omega(j - j_{in})], \quad (1)$$

where E_B is the binding energy per unit mass, $j = r^2\Omega$ is the angular momentum per unit mass, j_{in} is the specific angular momentum of matter accreted by the black hole, and Ω is the orbital frequency. To be precise, relativistic corrections should be applied to these quantities (Novikov & Thorne 1973, Page & Thorne 1974), but the Newtonian formalism expresses the physics more transparently.

If the torque is largely due to MHD turbulence in which the radial and azimuthal magnetic field components are correlated, this energy is initially given primarily to the field and secondarily to turbulent motions of the matter. In the simulations of HK02, for example, within the disk proper (i.e., well outside r_{ms}) the local ratio of magnetic field to random motion energy density varies from ~ 1 to ~ 100 . This energy is then transferred from relatively long lengthscale motions to shorter lengthscale motions in a turbulent cascade whose eddy turnover time (in the same simulations just cited) is typically comparable to an orbital period. By definition, the lengthscale at which the cascade cuts off is the lengthscale on which the dissipation rate becomes as fast as the nonlinear energy transfer rate. Under ordinary conditions, this may be many orders of magnitude smaller than the stirring scale. Consequently, the total time required to traverse the cascade would then be a logarithmic factor, perhaps $\sim O(10)$, times larger than the orbital period. However, when radiation pressure dominates gas pressure, photon diffusion may cut in at relatively large scales, particularly in regard to compressive modes (Agol & Krolik 1998). When that is the case, the multiplicative factor might be rather smaller. At the same time, not all of the energy has to be thermalized by the turbulent cascade; other losses may occur. Buoyancy, for example, causes magnetic flux to rise to the surface of the disk and escape. Because the underlying force is gravitational, the characteristic timescale for this motion is the orbital period, but fluid drag and the necessity of draining some of the attached matter can slow this process. Thus, we write $t_{turb} = \tau_{turb}P_{orb}$ and expect that τ_{turb} will be between a few and ~ 10 .

To determine the turbulence edge, we compare this cascade timescale to the inflow time. Well outside r_{ms} in a thin disk, the inflow time is always much longer than the turbulent cascade time. Indeed, this contrast is part of the separation of scales that makes it reasonable to parameterize the stress by α . However, the inflow time diminishes rapidly as the region of the marginally stable orbit is approached from the outside. One way to estimate the mean inflow time in that regime is via the equation of angular momentum conservation as applied to a statistically time-steady disk

$$\int d\phi \int dz T_{r\phi} = \dot{M}\Omega [1 - j_{in}/j], \quad (2)$$

where $T_{r\phi}$ is the r - ϕ component of the stress tensor. This equation may be rearranged to yield an estimate of the inflow time:

$$t_{in} = \frac{r^2 \int d\phi \int dz \rho}{\int d\phi \int dz \rho v_{r,r}} = \frac{r^2 \Omega [1 - j_{in}/j] \int d\phi \int dz \rho}{\int d\phi \int dz \langle B_r B_\phi / 4\pi \rangle}, \quad (3)$$

where ρ is the volume density, and we have assumed that all the angular momentum transfer is due to magnetic stress. Note that this estimate is actually the inverse of the density-weighted mean infall rate, rather than the density-weighted infall time. It also assumes that infall is limited solely by the rate at which angular momentum can be removed. It is most appropriate in the rotationally supported part of the disk, and is wholly inapplicable inside r_{ms} where, by definition, rotation cannot prevent infall.

In the conventional treatment (e.g. Abramowicz & Kato 1989), the stress is assumed to be $\simeq \alpha p$ for a constant $\alpha \lesssim 1$ and pressure p . Because the pressure decreases sharply as the flow accelerates inward near the marginally stable orbit, the stress falls equally sharply. The factor in square brackets in the numerator of the right-hand-side of equation (3), which approaches zero near the inner edge, is then nearly cancelled by the diminishing stress in the denominator. However, when the stress is due to MHD turbulence, it does not decline near r_{ms} , the ratio of stress to pressure is not a constant, and the inflow time as estimated by equation (3) becomes steadily shorter as the flow moves toward the marginally stable region from the outside (see fig. 1). The inflow time as estimated by the torque condition does not approach zero even at r_{ms} because $j_{in} \neq j(r_{ms})$ in the simulation.

Comparison of this estimate with one derived by computing a density-weighted mean of r/v_r shows that angular momentum removal by magnetic stress is, indeed, the primary determinant of inflow in the disk body, but infall no longer becomes angular momentum-limited at radii inside $\simeq 4r_g$ (we define the gravitational radius $r_g \equiv 2GM/c^2$). Inside r_{ms} , continued inflow can occur on the dynamical timescale without any change in angular momentum; even in the region not far outside r_{ms} , little torque is required, and other forces, even if small, can help push matter inward. Primarily because of the approach of j to j_{in} , the ratio of the infall time to the orbital period falls sharply inside $r = 10r_g$, dropping below 10 inside $r \simeq 7r_g$.¹ Because the turbulent cascade time is perhaps $O(10)$ orbital periods, this line of reasoning would suggest that the turbulence edge (in this simulation) is near $\simeq 7r_g$.

2.2. Magnetic Field Structure

Another approach to determining the turbulence edge is to look for a change in magnetic field structure that might result from the turbulence-dominated to flux-freezing transition. In the disk body, where turbulence dominates, the magnetic field structure is determined by a balance between stirring by the MRI and nonlinear processes that transfer energy to smaller scales, where the energy is ultimately dissipated. Although these nonlinear processes do not intrinsically lead to correlations between different field components, the linear properties of the MRI and the consistent sense of

¹Even in statistically steady disks, local fluctuations are so large that individual fluid elements can spend very different lengths of time traversing a given radial span. A more complete treatment would therefore consider the probability distribution for the infall time of matter at a given radius.

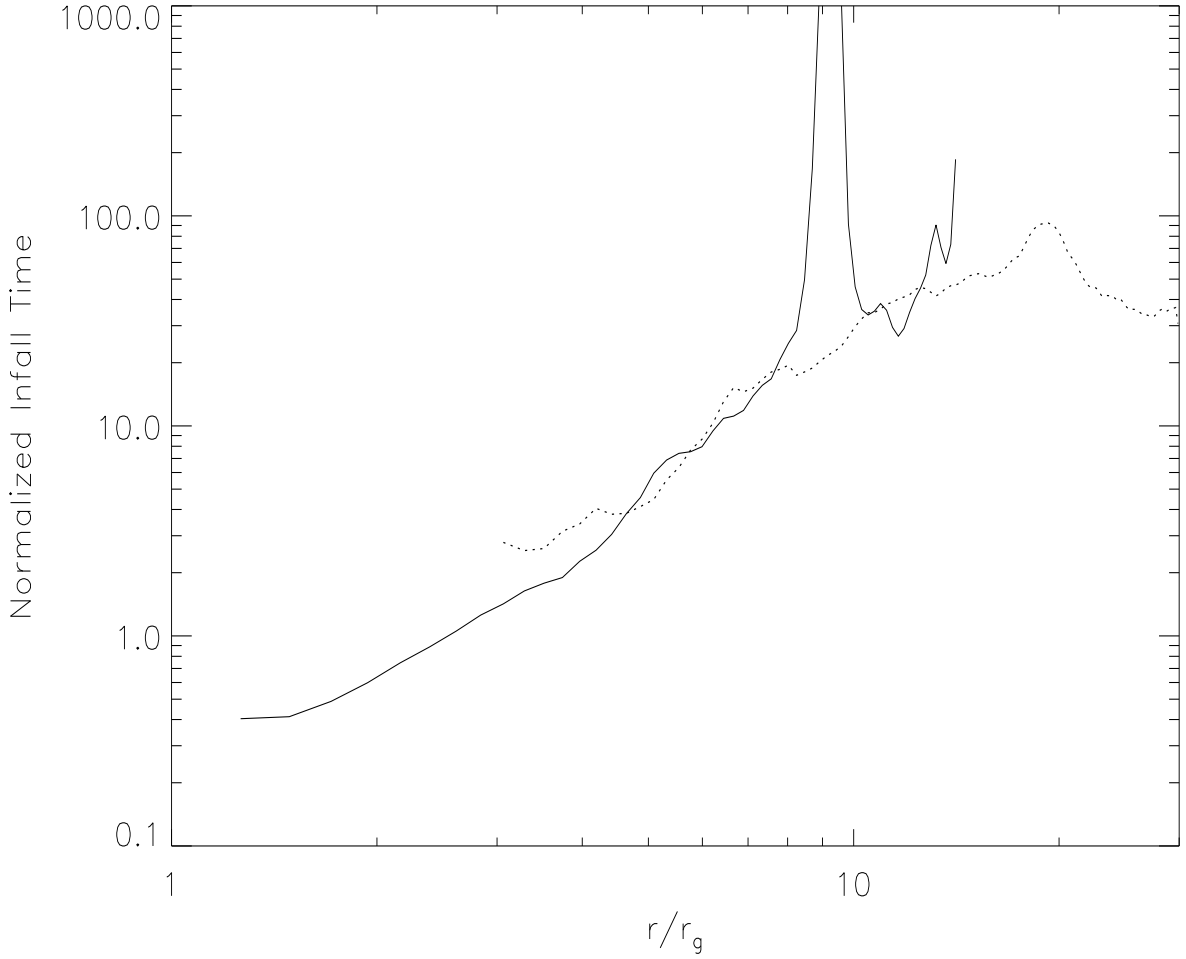


Fig. 1.— Mean infall time in units of the orbital period estimated two different ways. The solid curve shows the density-weighted mean value of $r/(v_r P_{orb})$ in a late-time snapshot from the high-resolution initially-poloidal simulation of HK02; the dotted curve shows the mean infall time as estimated by eq. 3 using data from the same simulation and setting $j_{in} = 0.95j(r_{ms})$, as indicated by the results of HK02. The spike in the solid curve near $r = 10r_g$ and that curve’s end near $r = 15r_g$ are both artifacts of the finite mass in the simulated accretion disk; at large radii, its material, in net, moves out.

orbital shear impose a correlation between B_r and B_ϕ such that $\alpha_{mag} \equiv \langle B_r B_\phi \rangle / \langle B^2 \rangle \simeq 0.25$ (Hawley, Gammie & Balbus 1996; HK01). Indeed, it is these correlated magnetic fluctuations that enable the MHD turbulence to serve as an angular momentum transport mechanism. On the other hand, where the flow is dominated by infall, so that the field evolution is best described by simple flux-freezing, orbital motion is the dominant factor and one would expect the shear to create a larger B_r – B_ϕ correlation. Thus, the radius inside which α_{mag} begins to grow above its characteristic turbulent value can mark the place where transfer of energy to small lengthscales becomes slower than infall.

To examine this in detail in the initially-poloidal simulation of HK02, we compute the density-weighted mean value of α_{mag} in a single late-time snapshot as a function of radius (Fig. 2). As the figure shows, α_{mag} begins to rise at radii less than $\simeq 6r_g$. The position of this rise fluctuates substantially from time to time. However, wherever the change begins, α_{mag} rises steadily inward until reaching a value near unity deep in the plunging region. In the initially-toroidal simulation of HK02, this transition occurs at rather smaller radius, always close to $3r_g$, but the rise inward of this point is, if anything, sharper.

2.3. Infall and turbulent velocities

In the heart of the accretion disk, fully developed MHD turbulence produces velocity fluctuations relative to the mean velocity that are substantially larger than the mean accretion velocity itself. As the flow approaches the inner edge, however, the accretion velocity increases relative to the fluctuations. Thus, another measure of the transition from the turbulence-dominated regime to the smooth infall regime is the ratio of the random velocity to the mean. As Figure 3 shows, this ratio is $\sim 5 - 10$ in the disk body, but begins diminishing near $r = 8r_g$ and falls $\propto r^2$ all the way into the plunging region. Near the inner edge of the simulation, the turbulent fluctuations are only $\sim 0.1\times$ the mean radial velocity.

2.4. Summary

Based on these estimates, we conclude that the turbulence edge in initially-poloidal simulations is in the neighborhood of $6 - 8r_g$, but may be closer to r_{ms} when the field is initially toroidal. For reasons discussed in HK02, it is likely that the initially-poloidal case is closer to reality than the initially-toroidal one, so one might expect the larger radius to be more representative of real disks.

If so, we may calibrate the factor τ_{turb} *post hoc*. Assuming that the turbulence edge is at $r \simeq 7r_g$, we see from Fig. 1 that $t_{in} \simeq 7P_{orb}$ at that point. By definition, $t_{in} \simeq t_{turb}$ at that radius, so we conclude that $\tau_{turb} \simeq 7$, in line with our expectations.

The position of the turbulence edge may be a function of disk thickness h , and/or the accretion

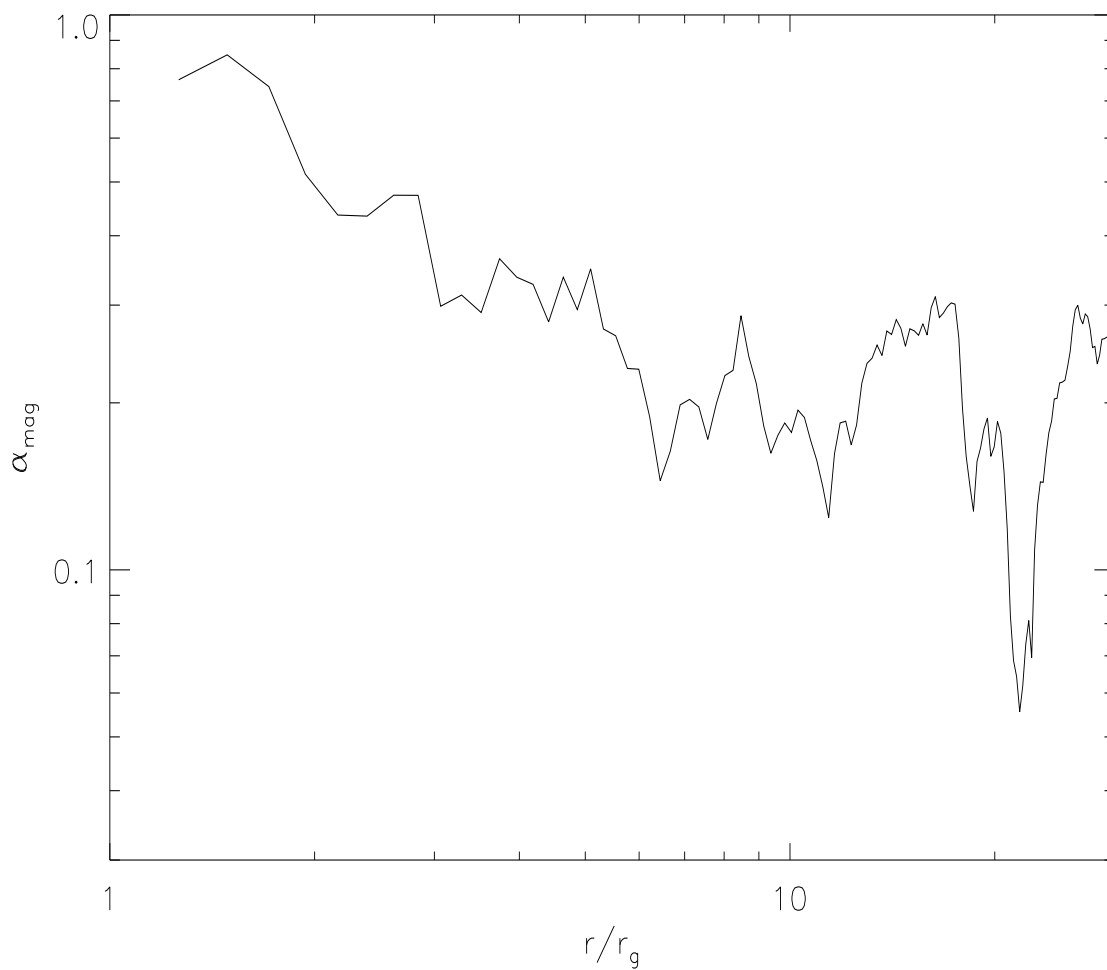


Fig. 2.— The density-weighted ratio of magnetic stress to magnetic energy density as a function of radius. Data are taken from the same set used for Figure 1.

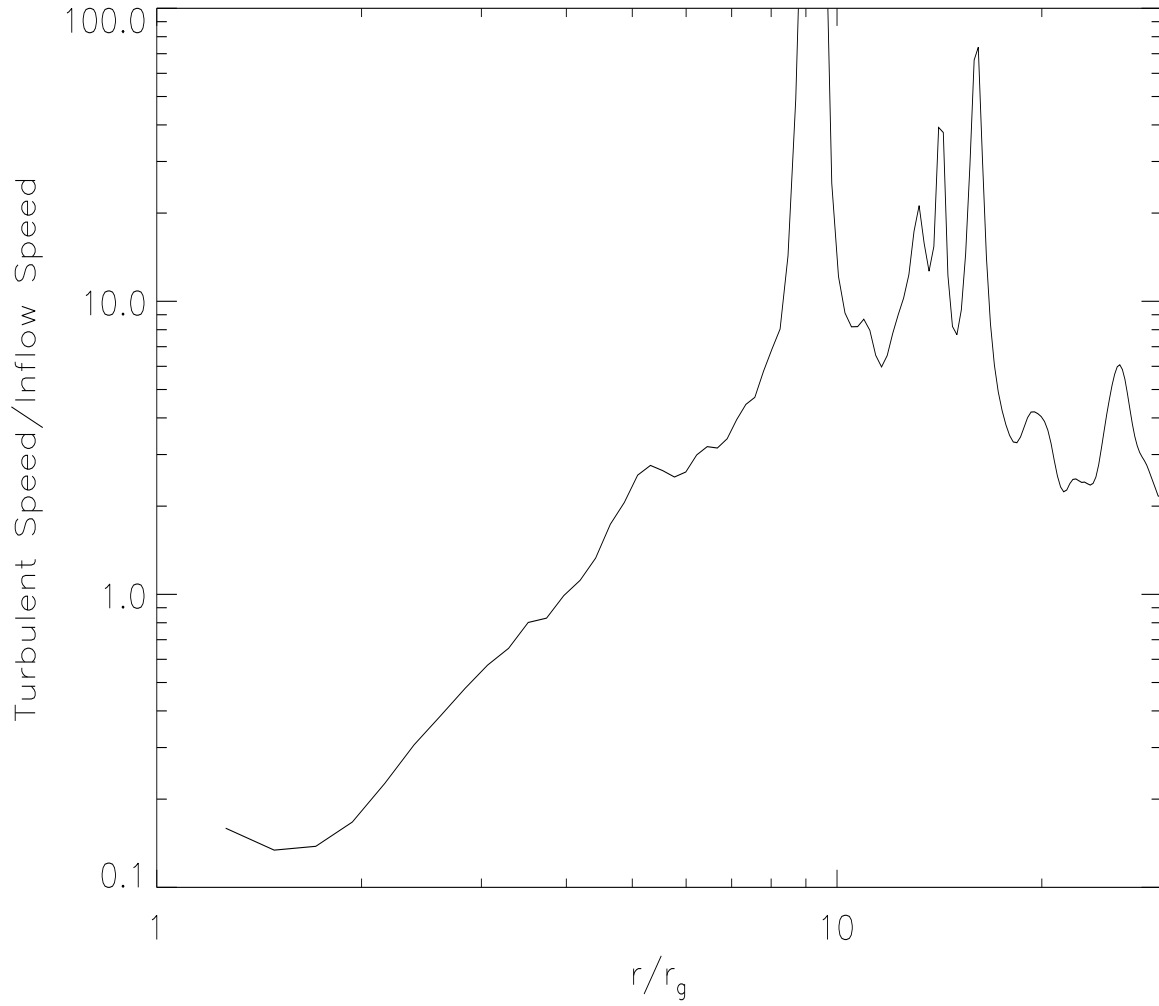


Fig. 3.— The ratio $v_{r,rms}/\bar{v}_r$, where \bar{v}_r is the density-weighted mean radial velocity and $v_{r,rms}$ is the density-weighted *rms* radial velocity fluctuation relative to \bar{v}_r . The data are from the same set used in Figures 1 and 2.

rate. The infall time t_{in} is always $\sim P_{orb}$ in the inner disk, but it increases to $\sim \alpha^{-1}(r/h)^2 P_{orb}$ in the disk body. Therefore, the infall time must rise more rapidly near $r \simeq 10r_g$ in cold, thin disks than in the simulated disks, which have $h/r \sim 0.1\text{--}0.2$. On this basis one would expect the turbulence edge to move to smaller radius for smaller h/r . Similarly, inward-directed pressure gradients can be significant within a distance h of r_{ms} , causing the final plunge to begin at a larger radius for hotter disks. However, there is little room for the turbulence edge to move too much closer to r_{ms} , so the dependence on h/r might be relatively weak.

3. The Stress Edge

3.1. General considerations

When matter crosses the event horizon of the black hole, it loses all ability to communicate with the outside world, even with signals traveling at c . If the accretion flow were time-steady and spherically symmetric, it would be easy to define an analogous surface, *the stress edge*, where a more restricted loss of communication takes place: the surface where dynamical communication ceases. That is the surface on which the inflow speed (as measured, for example, by a distant observer) exceeds the magnetosonic speed (measured relative to the same observer).

In real accretion flows, which are thoroughly non-steady and non-symmetric, it becomes much harder to define such a surface. Even in steady flows, asymmetry significantly complicates the issue. Imagine, for example, a steady flow in which the magnetosonic surface has a dimple. It would be entirely possible for signals to travel diagonally inward within the super-magnetosonic region, cross the boundary into the sub-magnetosonic region, and travel outward from there. When that happens, the magnetosonic surface is no longer a final boundary beyond which the flow loses causal contact with the outside world. The surface on which that takes place lies somewhere closer to the black hole; its exact location depends on details of the flow structure.

If the flow is non-steady, which is the realistic case, individual asymmetric structures like the one described in the previous paragraph are the norm, but with the additional complication that they are transient. Causal paths need exist only for the time the signal travels through them. Time-variation might be so violent that time-averages would erase any indication that such paths exist. The only way to determine these causal trapping surfaces for certain is to trace all characteristics through spacetime to their end, either in the black hole or back to the outside. For all these reasons, the concept of an average stress edge is perhaps the least well-determined of all the edges discussed here.

Giving up hope of defining this edge exactly, instead we attempt to locate it approximately using two crude indicators: the ratio of infall speed to magnetosonic speed, and gradients in the matter's angular momentum and energy.

3.2. Comparing the magnetosonic and infall speeds

As was just discussed, the point where the infall speed becomes equal to the magnetosonic speed clearly demarks the stress edge only in spherically-symmetric, time-steady flows. Nonetheless, we might look to this ratio as giving at least a crude estimate of this edge’s position. Fig. 4 shows an azimuthal average of this ratio at a particular late-time instant in the initially-poloidal simulation of HK02. In this snapshot, the surface within which the infall speed is generally greater than the magnetosonic speed falls roughly between 2.5 and $3r_g$ between the midplane and $z \simeq +r_g$, but slants radially inward below the equatorial plane. Thus, from this sort of data, one might imagine the stress edge as occurring at a variety of radii between 2 and $3r_g$, depending on altitude. The asymmetry between regions above and below the midplane is, of course, time-variable. Inside the disk body (i.e., $r \geq 3.5r_g$ and $|z| \lesssim 0.1r$), the mean infall speed is a tiny fraction of the magnetosonic speed.

Next, we consider this ratio in the equatorial plane as a function of time. After $t = 1000$, when the accretion flow has established a quasi-steady state, the location where v_r becomes super-magnetosonic remains inside r_{ms} , but varies rapidly, from a minimum at $r = 2.3r_g$ out to a maximum near $r = 2.9r_g$. We expect that there are also similarly large fluctuations in the location of the magnetosonic surface away from the equatorial plane.

3.3. Specific angular momentum

A contrasting perspective is given by the variation in specific angular momentum across the accretion flow (fig. 5). As this figure shows, $\langle \partial j / \partial r \rangle > 0$ all the way to the inner edge of the simulation problem area at $r = 1.25r_g$. In the equatorial plane, the specific angular momentum continues to fall at least as far inward as $r \simeq 1.5r_g$. Away from the midplane, the azimuthally-averaged poloidal velocity field angles toward the equatorial plane, but not as steeply as the angular momentum contours; hence, the angular momentum of individual fluid elements falls as they flow inward. If this figure were our only diagnostic of the stress edge, we might conclude that this edge lies inside the smallest radius treated in this simulation, i.e. at less than $1.25r_g$.

3.4. Relation to turbulence edge

For a third estimate of the stress edge’s location, we examine its relation to the turbulence edge. The stress edge must be inside the turbulence edge for it must occur where the net inflow velocity dominates over the velocity fluctuations. Moreover, because conditions at the turbulence edge provide a sort of boundary condition for the relatively predictable behavior in the flux-freezing region, we can use a simple analytic argument to estimate how far inside the turbulence edge the stress edge occurs. In essence, this argument is the same as the one employed in Krolik (1999a).

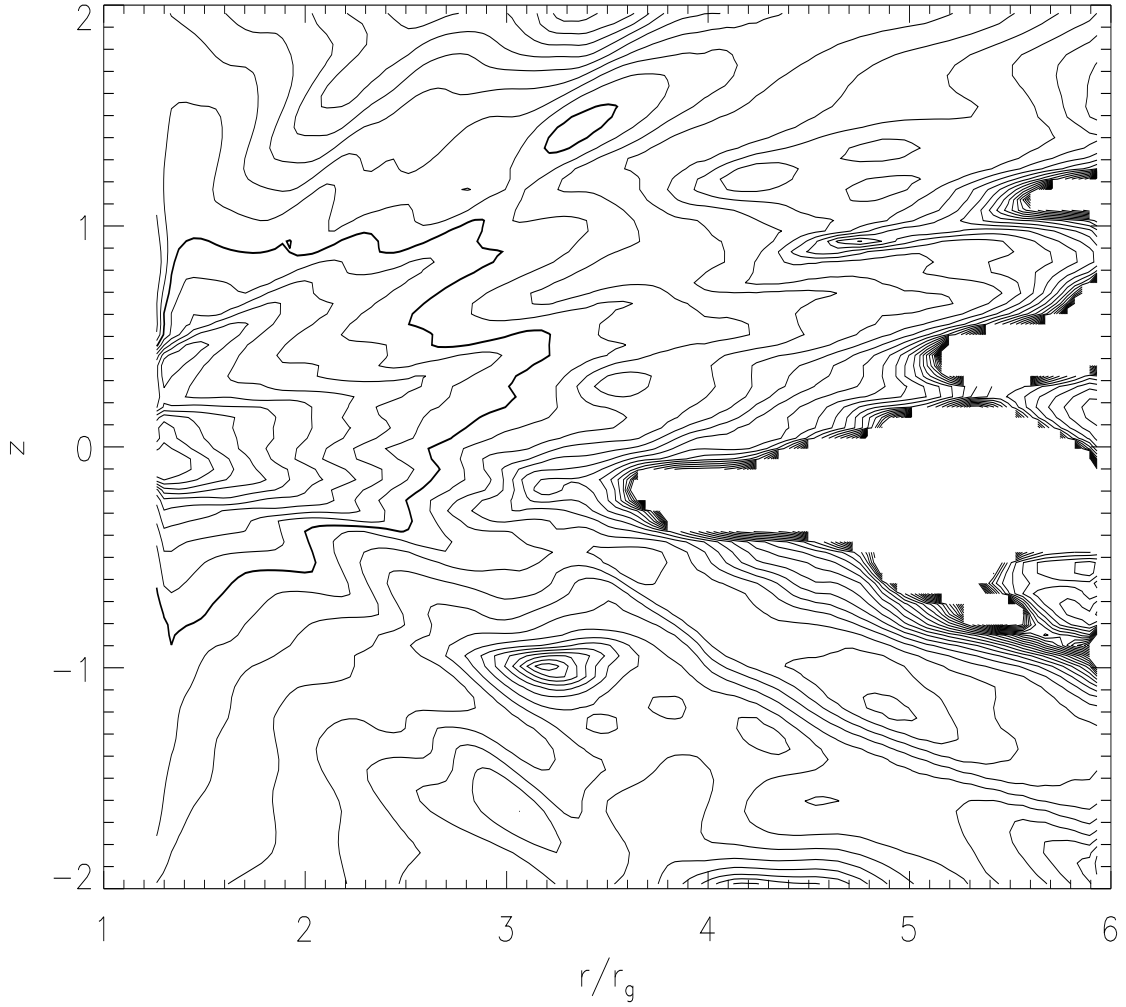


Fig. 4.— Azimuthal average of the local ratio of infall speed to magnetosonic speed at late time in the initially-poloidal simulation of HK02. Contours are logarithmic, spaced every 0.1 dex. The heavy contour cutting the equatorial plane near $r = 2.5r_g$ marks the instantaneous azimuthally-averaged magnetosonic surface. Where the contours disappear inside the disk body, the mean ratio of infall speed to magnetosonic speed is less than 10^{-3} .

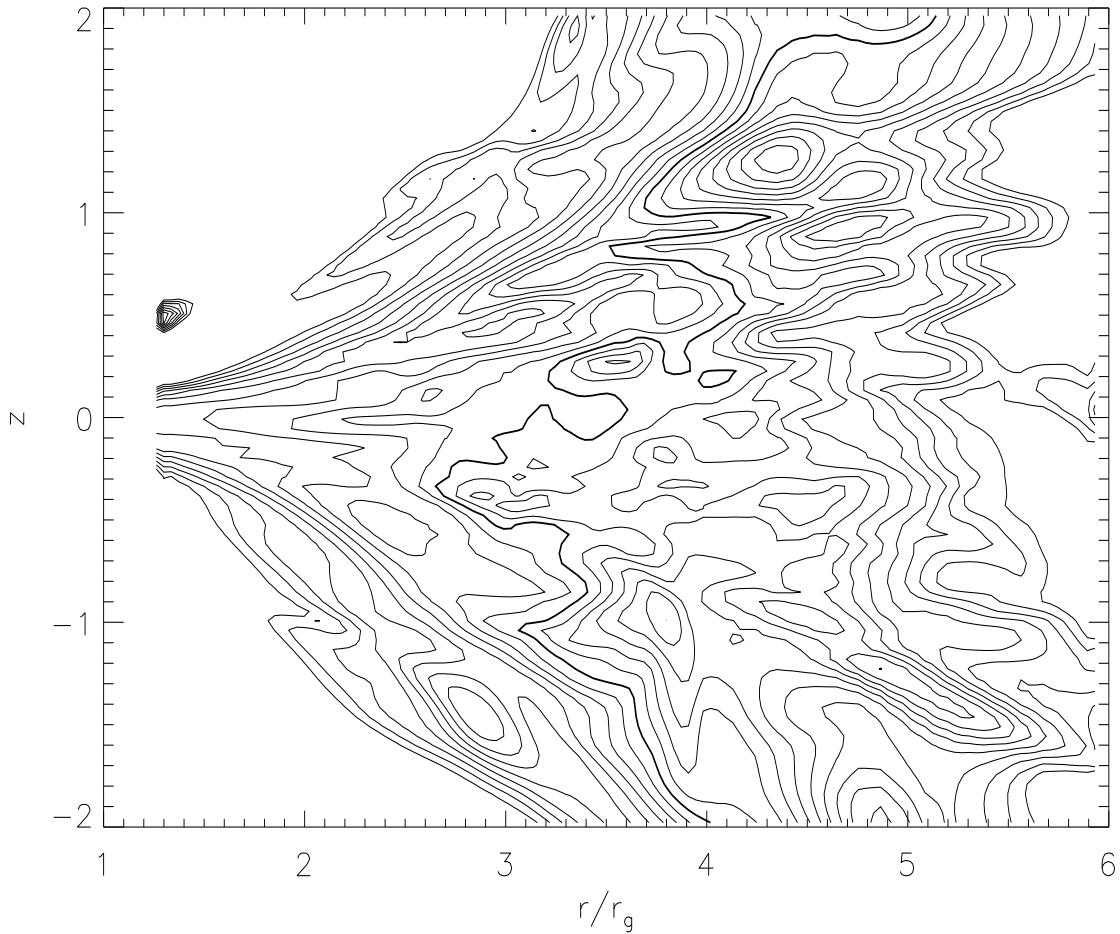


Fig. 5.— Azimuthal average of the the specific angular momentum at the same late time as Fig. 4 in the initially-poloidal simulation of HK02. Contours are linear, spaced by 0.03 in units of $\sqrt{2}GM/c$. The heavy contour marks the specific angular momentum (2.60) of the marginally stable circular orbit.

Our reasoning begins with equation (2), evaluated at the turbulence edge and assuming that all the stress is magnetic. This condition fixes the magnetic field intensity at the turbulence edge. Extrapolating the field strength to smaller radii with the assumption of flux-freezing then gives an estimate of the Alfvén speed. Writing all quantities evaluated at the turbulence edge with a subscript $*$ and introducing mass-conservation in the form $2\pi r h \rho v_r = \dot{M}$, we find

$$\frac{v_A}{v_r} = \left\{ \frac{2}{\alpha_{mag*}} \frac{\langle B^2 \rangle}{\langle B^2 \rangle_*} \frac{r h}{r_* h_*} \frac{v_{\phi*}}{v_r} [1 - j_{in}/j_*] \right\}^{1/2}, \quad (4)$$

where v_ϕ is the azimuthal speed. To verify equation (4), we plot (in fig. 6), the left hand and right hand sides of this equation for the inner region of the initially poloidal simulation from HK02. The values are averaged over height, angle, and time from $t = 1000$ to 1830 (the endtime). If we set $\alpha_{mag*} = 0.3$, we find that the simulation data give a very close match to this analytic prediction for r_* between ~ 6 and $8r_g$; The figure uses $r_* = 6.3r_g$, a number well within the range previously estimated for the turbulence edge.

Supported by this check, we may then use equation (4) to estimate the position of the magnetosonic surface based on conditions at the turbulence edge, once again using that surface as a rough guide to the location of the stress edge. Because the simulations also suggest that the height-integrated magnetic energy doesn't change much as a function of radius in this region, the definition of the stress edge r_s based on equation (4) simplifies to

$$r_s \simeq \left[\alpha_{mag*} \frac{j_{in}/j_*}{1 - j_{in}/j_*} \frac{v_r(r_s)}{v_\phi(r_s)} \right]^{1/2} \simeq \left[\frac{v_r(r_s)}{v_\phi(r_s)} \right]^{1/2}. \quad (5)$$

The simplified form reflects the simulational results that $\alpha_{mag*} \simeq 0.3$ and $j_{in}/j_* \simeq 0.8$. This form demonstrates that $r_s < r_{ms}$ because v_r/v_ϕ is generally still a small number until well inside r_{ms} . For example, for the data shown in Figure 1 the mass-weighted mean $v_r/v_\phi \sim 0.1$ at r_{ms} , so that $r_s \simeq r_*/3 \simeq (2 - 2.5)r_g$. We emphasize, however, that the location of the turbulence edge fluctuates with time, causing movement of the stress edge. A relation such as equation (4) holds in an approximate and time-averaged sense.

4. The Reflection Edge

The edges discussed above are dynamical. Other interesting edges have to do with the innermost places from which observable photons may emerge.

Many accreting black holes exhibit Compton reflection features. These are broad bumps in the spectrum from $\simeq 10$ to $\simeq 50$ keV. All photons can be reflected by Compton scattering from ionized material, but those with energy below $\simeq 10$ keV are more likely to be absorbed by a variety of photoelectric processes, while those with energy ~ 100 keV or more lose energy to Compton recoil in the very process of reflection (Lightman & White 1988). To produce a Compton reflection feature,

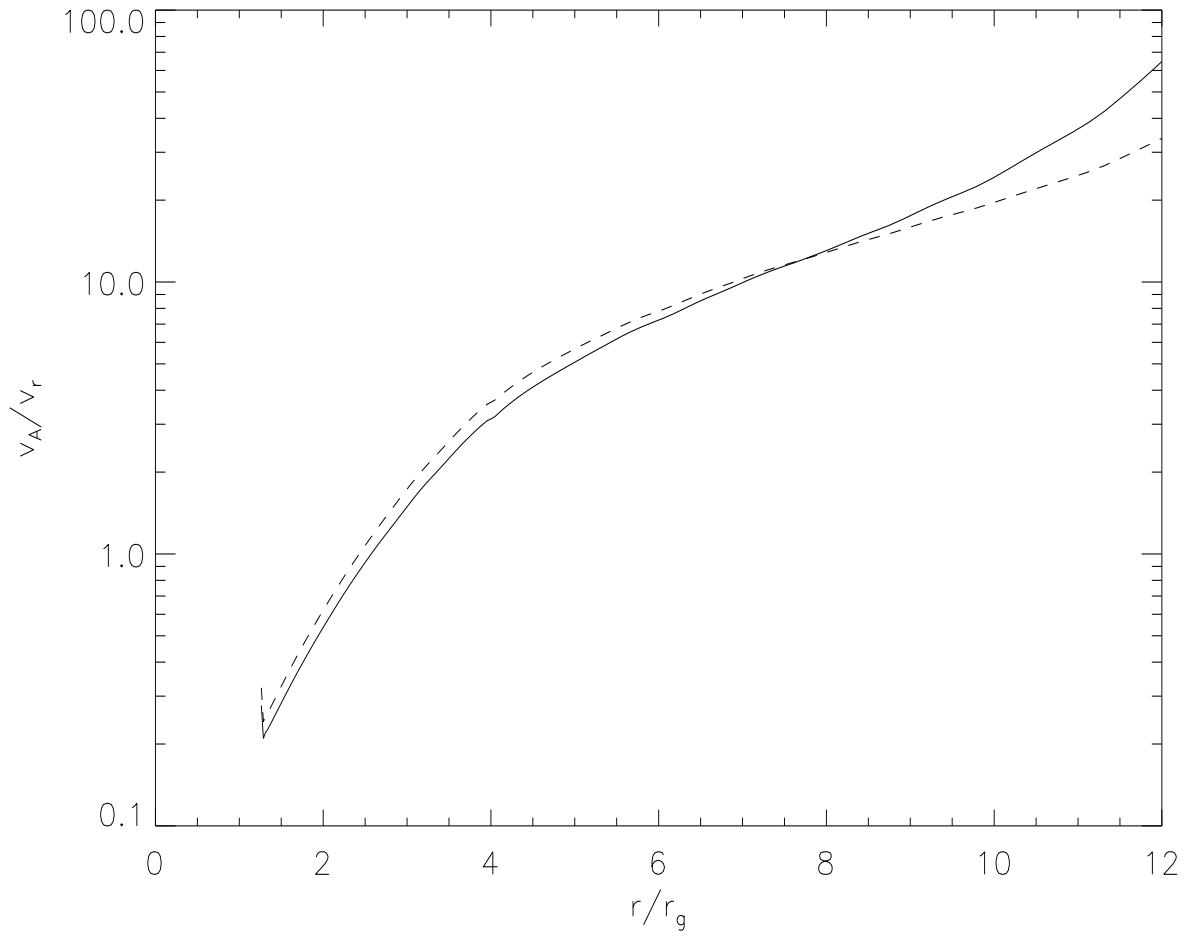


Fig. 6.— Plot of the ratio of the Alfvén speed to the infall velocity (solid line), and the right hand side of equation (4) (dashed line).

accretion disks must satisfy two criteria: they must be optically thick to Compton scattering, and their matter must not be too ionized.

Two very similar criteria regulate Fe $K\alpha$ production in disks. This emission line can be generated when hard X-rays illuminate matter containing unstripped Fe atoms and ions. When the Fe is less ionized than H-like or He-like, the line is produced by fluorescence; in the higher ionization stages, the process is actually recombination, but it scales in identical fashion with illuminating flux until most Fe atoms are fully stripped of their electrons.

Because the Fe $K\alpha$ line and the Fe K-edge that dominates the low-energy end of the Compton reflection feature can be shifted in energy by general relativistic effects, their location in X-ray spectra can provide direct diagnostics of orbital properties deep in the relativistic potential. It is therefore very important to correctly identify their origin.

Although it is common to assume that this *reflection edge* is identical to the marginally stable orbit, Reynolds & Begelman (1997) pointed out that this is not necessarily the case because material farther in could be illuminated by hard X-rays generated elsewhere. On the other hand, Young et al. (1998) questioned whether there would be enough unstripped Fe in the lower-density material in the plunging region to efficiently produce fluorescence photons. The fractional abundance of unstripped Fe is controlled by the ratio J_x/ρ , where J_x is the mean intensity of X-rays with energy > 7 keV. When J_x/ρ is too great, the efficiency of $K\alpha$ production falls because an increase in the illuminating flux no longer produces any increase in line photon emission. In addition, because the Fe K-edge photoionization opacity of matter with a solar abundance of Fe is approximately the same as the Thomson opacity, illuminating photons are only fully used when the column density is great enough to make the matter Compton thick. Thus, the falling density in the plunging region reduces the $K\alpha$ emission efficiency for both these reasons.

One of the most noteworthy results of the MHD simulations is to show that, particularly in the plunging region, accreting matter fluctuates widely in density, in both space and time. Regions separated by less than the azimuthally-averaged scale height can differ in density by factors of 10–30. As a result, the optical depth at fixed radius can vary in azimuth by factors of 2–3. A treatment that assumes all the accreting matter has the same mean density and optical depth could therefore miss important effects.

In our simulations, we have no way of estimating the hard X-ray intensity, and, because we have no definite unit of density, we can measure the gas density and column density only in relative terms. However, by normalizing the mass inflow rate to the Eddington rate, we can make a correspondence between the density in the simulation and a physical density. In physical units, $\dot{M} = 1.7 \times 10^{17} (\dot{m}/\eta) M/M_\odot \text{ gm s}^{-1}$, where \dot{m} is the mass inflow rate in Eddington units and η is the “efficiency” factor, i.e., the fraction of the rest-mass energy available for radiation.

Figure 7 shows the value of the surface density Σ as a function of radius for the inner region of the poloidal field simulation of HK02. The solid line is the azimuthally-averaged value and the dashed lines are the minimum and maximum values. The inflow stream has a prominent $m = 1$

spiral pattern, and the minima and maxima provide a measure of the variation with angle. The values are normalized to the average value at r_{ms} .

The surface density Σ , and with it the optical depth, decline smoothly inward, dropping by a factor of ~ 10 from r_{ms} to the inner boundary and increasing roughly proportional to $r^{3/2}$ out to $r = 10r_g$. The drop in the plunging region is less severe than in Figure 1 of Reynolds & Begelman (1997) because they make the artificial assumption that the infall velocity goes to zero at r_{ms} . In contrast, we observe no sharp change because our infall velocity varies smoothly across r_{ms} .

The initially toroidal simulation from HK02 shows a steeper inward decline in Σ , which is roughly proportional to r^3 out to $r = 10$. Even here, however, there is no sudden break or change in character at $r = r_{ms}$.

Employing the conversion factor defined above, we find that the average Σ at r_{ms} in the poloidal simulation is $14(\dot{m}/\eta)$ gm cm $^{-2}$. The corresponding mean Thomson optical depth is $\tau_T \simeq 5(\dot{m}/\eta)$. In other words, at high accretion rate, all of the stably-orbiting part of the disk and some of the plunging region are Thomson thick, but at low accretion rate, even the inner part of the stable disk may be optically thin. The reflection edge may therefore lie on either side of r_{ms} , depending on the accretion rate. This conclusion is at variance with standard analytic models for accretion disk equilibria because, unlike them, we allow for the smooth acceleration in the radial inflow speed that begins outside the marginally stable orbit.

Although the mean column density does decrease inward, the maximum volume density in the inflow spiral remains roughly constant until $\sim 2r_g$, before dropping. Of course, the maximum fills an increasingly small volume, but assuming a constant incident X-ray flux, the persistence of local high-density regions means that there can be some material deep in the plunging region that is no more highly-ionized than it was at the marginally stable orbit.

Finally, we comment that the reflection edge is, in some respects, the nearest analog to what one might ordinarily define as the disk’s inner edge. It is the place where the integrated surface density has declined enough that the disk becomes effectively transparent.

5. The Radiation Edge

The previous section discussed photon reflection; no reflection can happen, of course, unless photons are generated to be reflected. Thus, we are led to the last edge we consider, the *radiation edge*, the innermost radius from which significant radiation emerges. There are two main considerations in establishing this edge: the heating that takes place in the plasma, and the rate at which that heat can be radiated away.

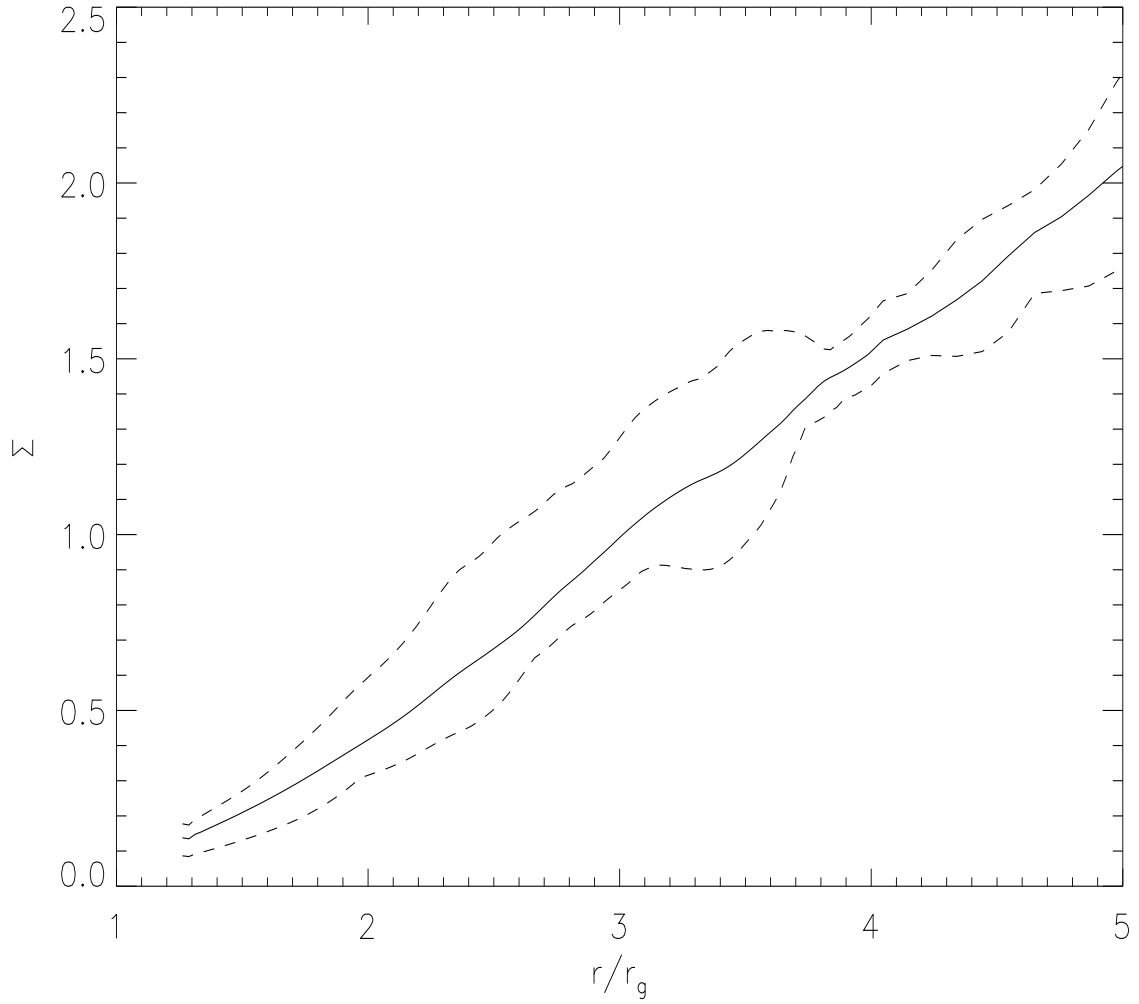


Fig. 7.— Plot of surface density Σ as a function of radius in inner disk. The solid line is the azimuthally-averaged value, normalized to unity at r_{ms} . The dashed lines are the maximum and minimum values at each radius.

5.1. The dissipation distribution

Outside the stress edge in a time-steady disk, the amount of energy available for local dissipation is the difference between the net rate of change in the matter’s binding energy and the energy that it loses by doing work through stresses on adjacent matter (eqn. 1). Conventional Novikov-Thorne models assume a boundary condition on the stress that forces dissipative heating to end at the marginally stable orbit (Novikov & Thorne 1973, Page & Thorne 1974). As first suggested by Krolik (1999a) and confirmed in the simulations of HK01 and HK02, stress due to MHD turbulence continues right through the marginally stable region and well into the plunging region. Consequently, it cannot be assumed that dissipation—and therefore radiation—end abruptly at r_{ms} .

One way that the dissipation distribution may be altered from the Novikov-Thorne prediction is for the extra stresses in the inner part of the accretion flow to convey energy coherently from plunging matter back to the disk proper, where it can then be dissipated. Agol & Krolik (2000) showed how a stress expressed at r_{ms} translates into an extended dissipation distribution at more distant radii. Close outside r_{ms} the dissipation per unit area drops very rapidly with increasing radius; at somewhat larger radii, it scales $\propto r^{-7/2}$.

The Agol & Krolik solution refers to the vertically-integrated dissipation rate. Because it is based only on energy conservation, it has nothing to say about the vertical distribution of that dissipation within the disk. For the purpose of making more specific spectral predictions, that distinction is important. In particular, the radial emissivity of reflection features (as discussed in the previous section) depends on the coronal dissipation rate. We will return to this point in §6.

A second alteration to the classical dissipation distribution may occur in the plunging region itself. Independent of how much energy may be transferred from there to the disk body, there can be very large local energy exchange between adjacent fluid elements. For example, in the initially-toroidal simulation of HK02, there are places in the plunging region where material with binding energy twice the mean finds itself a small fraction of a radius from material that has very nearly zero binding energy. Some of the energy involved may find itself dissipated. In addition, stripes of oppositely-directed magnetic field can be brought very close together, offering opportunities for rapid reconnection. Because the field energy is large compared to the pressure in this region, the heating associated with reconnection could be quite important.

5.2. Photon generation and escape

The stress distribution in the inner region of an accretion disk also cannot automatically be transformed into a radiation distribution. Any of several effects could cause inefficiency in the transformation of energy into heat and thus into escaping photons. One possibility, which has been the focus of a great deal of attention in recent years, is that the primary dissipation mechanism

heats the ions, but not the electrons (Rees et al. 1982; Narayan & Yi 1995). In the present discussion, we will not consider that possibility, except to note that to answer the question of which species receives the majority of the heat will require detailed consideration of the small-scale processes that terminate the nonlinear cascade of the MHD turbulence. Here we will assume that $T_{ion} = T_e$. Another plausible alternative channel for energy loss is mechanical work. This channel has two branches: organized outflows such as winds and jets, and simple $p dV$ work within the accretion flow. A third possibility is that the inflow may be so rapid that there is not enough time for the matter to generate photons, and for the photons to diffuse out, before the fluid reaches the black hole (Abramowicz et al. 1988). Here we will concentrate on the latter three issues: adiabatic cooling, photon generation, and photon diffusion.

One might expect adiabatic cooling to become more important than dissipative heating when the inflow time becomes shorter than the time to dissipate the MHD turbulence, i.e., inside the turbulence edge, but there are two loopholes in this line of reasoning. The first is whether the gas actually falls in density as it plunges inward. If all that happened were an increase inward of $|v_r|$, a sharp density drop would be inevitable. However, as seen in the simulations of HK01 and HK02, and as discussed above in §4, the density in the spiral inflow can remain higher than what might be predicted. Convergence to the equator and into a nonaxisymmetric spiral can compensate for inward acceleration.

The second loophole is that the turbulence edge is defined specifically in terms of the turbulent cascade of magnetic energy to short lengthscales. Other, more rapid, forms of dissipation can also occur, such as shocks and magnetic reconnection. In particular, in the simulations of HK02 there are enough weak shocks that the specific entropy (defined as $p/\rho^{5/3}$) rises by roughly a factor of 5 from $r = 6r_g$ to $r = 1.25r_g$ in the equatorial plane. As a result, the temperature actually rises slightly with decreasing radius in this region. Because this simulation does not capture several other sources of heating (notably numerical magnetic reconnection), the heating recorded is probably an underestimate.

In most—but not all—circumstances, the photon generation time is shorter than the photon diffusion time. To illustrate the range of possibilities, we consider two cases, one in which the primary radiation mechanism is bremsstrahlung, the other in which the primary mechanism is inverse Compton scattering.

First consider bremsstrahlung. It is slowest relative to the infall time if the gas is essentially in free-fall. When that is a good description,

$$\frac{t_{brems}}{P_{orb}} = \frac{1}{9\alpha_{fs}[\ln(kT/m_e c^2) + 1.5]} \frac{\eta}{L/L_E} \frac{h}{r} \frac{v_r}{v_{ff}}, \quad (6)$$

where t_{brems} is the characteristic time to radiate the gas’s thermal energy by bremsstrahlung, the numerical factors incorporate an approximation to the relativistic bremsstrahlung Gaunt factor, α_{fs} is the fine-structure constant, and v_{ff} is the radial free-fall speed (see, e.g., Krolik 1999b for the bremsstrahlung radiation coefficient written in this notation; note, too, that this expression

assumes a pure electron-proton plasma). Thus, when the accretion flow is geometrically thick and close to free-fall, the bremsstrahlung photon generation time is longer than an infall time in the plunging region, particularly for low accretion rate relative to Eddington. However, when the flow is slower, the photon generation time can easily be shorter than t_{in} .

In the initially-poloidal simulation of HK02, $h/r \simeq 0.1$ throughout the plunging region. The time- and mass-averaged mean inflow velocity v_r varied from $0.01v_{ff}$ at $r = 7r_g$ to $0.35v_{ff}$ at $r = 2r_g$. At late time, the mass-averaged temperature ($kT \propto p/\rho$) rises inward from $0.001c^2$ at $r = 10r_g$ to $0.004c^2$ at $r = 2r_g$. Using equation (6), we would then predict that the time required to radiate the gas's thermal content by bremsstrahlung is $0.008\eta(L/L_E)^{-1}P_{orb}$. Thus, bremsstrahlung cooling is rapid compared to the dynamical time so long as the accretion rate is greater than $\sim 10^{-2}$ the Eddington rate.

Bremsstrahlung is not the only plausible cooling mechanism; Compton cooling generally dominates when the electron temperature is substantially greater than the Compton temperature, $1/4$ the intensity-weighted photon energy, and the electron density is relatively low. Compton cooling is especially likely to be important when dissipation occurs within the plunging region. The characteristic energy loss time for this mechanism is

$$\frac{t_{Compt}}{P_{orb}} = \frac{9}{32\pi} \frac{m_e}{\mu_e} \frac{(r/r_g)^{1/2}}{L(x)/L_E}, \quad (7)$$

where μ_e is the mass per electron (generally $\sim m_p$) and $L(x)/L_E$ is the luminosity produced inside radius x , relative to Eddington. Unless $L/L_E \ll 1$, the Compton time remains much shorter than an orbital period throughout the (inner) portion of the disk that radiates nearly all the light.

On the other hand, depending on location, the diffusion time can be either much longer than an orbital period or rather shorter. In the disk body, the diffusion time is generally $\sim \alpha^{-1}P_{orb}$. However, as we have already estimated, the surface density, and hence vertical optical depth of the disk, diminishes smoothly through the inner part of the accretion flow, and, depending on parameters, the flow may become optically thin to Compton scattering either inside or outside r_{ms} . Where the disk is optically thin, photon scattering is unimportant; where it is optically thick, the diffusion time is $\sim \tau_T^2(h/r)(r/r_g)^{-1/2}P_{orb}$.

On the basis of these estimates, we conclude that the radiation edge of sub-Eddington disks is primarily determined by the total (i.e. turbulent plus shock plus reconnection) dissipation distribution. Where inflow is slow enough that the optical depth is large, t_{in} is longer than the radiation time; where inflow is faster, the optical depth falls sufficiently to permit efficient photon escape. Thus, if the flow inside the turbulence edge is laminar, the radiation edge will be located at most a short distance inside the point where most dissipation ceases. If there is dissipation at small radii, the disk could remain bright close to the black hole.

6. An observational application: Fe K α profiles

The emissivity of reflection features—both the “Compton bump” and Fe fluorescence—is determined by a combination of the different mechanisms that set the locations of the radiation and the reflection edges. Most efforts to infer the reflection emissivity have concentrated on Fe K α , so we will focus on that feature here.

Almost all phenomenological inferences of the K α emissivity have assumed that the inner edge of emission is identical with r_{ms} . For example, Nandra et al. (1998), fit their ASCA data from a number of Seyfert galaxies to a model for which the emissivity $j_{K\alpha} \propto r^{-\beta}$ for $r \geq 6GM/c^2$ (r_{ms} for $a/M = 0$) and zero inside that radius. For their sample, they found a mean value of $\beta \simeq 2.5$. Wilms et al. (2002) fit their K α profile from MCG –6-30-15 to a similar model, but with the inner radius and a/M variable. They found that $4.3 \lesssim \beta \lesssim 5$, and, by arguing that the inner edge of emission could be identified with r_{ms} , placed a lower bound on a/M .

Now that we can begin to distinguish between the radiation and reflection edges and the marginally stable radius, it is necessary to approach these inferences more circumspectly. As has already been discussed in §5, the coronal radiation edge—the version of the radiation edge relevant to driving X-ray fluorescence—could fall on either side of r_{ms} .

Whether reflection ceases inside or outside r_{ms} depends largely on the accretion rate. Thus, one could interpret extremely broad and red-shifted Fe K α profiles in either of two generic ways:

High accretion rate: If $\dot{m}/\eta \sim 1$, the reflection edge can be well inside r_{ms} . In this case, the lower bound on a/M suggested by Wilms et al. (2002) would not apply because many of the observed line photons could be created at $r < r_{ms}$. Reflection requires irradiation, and to have sufficiently strong irradiation in the plunging region, there must be either violent reconnection in that zone or strong coronal emission just outside r_{ms} . As shown by Agol & Krolik (2000), when extra torque is applied to the disk at some radius $r_t \geq r_{ms}$, the associated supplemental dissipation is concentrated very tightly at radii just outside r_t . In terms of Boyer-Lindquist coordinates, the dissipation rate falls especially steeply outside r_t when a/M approaches unity.

Low accretion rate: If $\dot{m}/\eta \ll 1$, the reflection edge is likely to move well outside r_{ms} . In the picture of accretion disks commonly adopted for line profile-modeling, the column density of matter rises so sharply near r_{ms} that disks are all optically thick at any radius $r \geq r_{ms}$. However, as Figure 7 shows, this is not so; the rise of optical depth with radius is relatively smooth, so that disks can easily be optically thin well outside r_{ms} , especially when \dot{m}/η is small. In this case, the lower bound on a/M posed by the prerequisites for creating this sort of profile become quite stringent, and might become impossible to satisfy.

Both interpretations share one conclusion: in order to excite enough K α emission at small enough radius to replicate the observed broad profiles, it is necessary to extend the range of disk (coronal) radiation well inward from the point where the Novikov-Thorne model predicts that dissipation becomes weak. If the K α photons were excited by hard photons produced locally whose

emissivity followed the Novikov-Thorne dissipation distribution, $j_{K\alpha}$ would be very small near r_{ms} , rise to a peak at significantly larger radius—in terms of Boyer-Lindquist radii, $r_{peak} \simeq 1.6r_{ms}$ for $a/M = 0$, and $1.2r_{ms}$ for $a/M = 0.998$ —roll over gradually, and then ultimately fall $\propto r^{-3}$. The sorts of crude fits already in hand make it clear that this sort of pattern for $K\alpha$ emissivity will not do—there must be additional emissivity at small radii.

7. Conclusions

The arguments presented here have shown how the simple term “disk inner edge” fragments into multiple meanings when accretion flows around black holes are examined carefully and quantitatively. At least four different definitions might be interesting, two referring to dynamical properties and two to observational ones. Moreover, even when one searches for an inner edge that is clearly defined conceptually, in a real disk what one is likely to find is a fuzzy, asymmetric border that varies in time.

The outermost inner edge is likely to be the turbulence edge, the place where the magnetic field ceases to be described by a balanced turbulent cascade and is better thought of as evolving through flux-freezing as the plasma that carries it flows inward. If the initially-poloidal simulation of HK02 is any guide, this occurs at $6\text{--}8r_g$ from the center of the black hole. This edge marks an important transition in the character of disk dynamics, from the familiar regime in which $t_{in} \gg t_{th} \gg P_{orb}$ ($t_{th} \sim \alpha^{-1}P_{orb}$ is the thermal time) to a quite different one in which all three timescales are comparable.

The other inner edge relevant to dynamics is the stress edge: matter inside this edge cannot communicate energy or angular momentum to matter outside. We demonstrated that the stress edge should, in general, lie well inside the turbulence edge, but it is difficult to locate unambiguously, as it is particularly strongly affected by time-variability and departures from symmetry. The position of this edge is central to accretion studies because it regulates what are arguably the two most important parameters of the system: the total energy and angular momentum removed from the accreted material before it enters the central black hole. Note that because the stress edge is well inside the turbulence edge, much of the energy released by accretion occurs in circumstances quite different from those in the disk body.

The reflection edge is the innermost material capable of producing a significant Compton reflection feature or Fe $K\alpha$ fluorescence. Because of the large fluctuations in gas volume and column density that occur in the plunging region, this edge may not even be a clean surface; rather, it may be that reflecting material breaks up into “islands” which become smaller and less common toward smaller radii. Normalizing the column density of matter in the simulations of HK02 in terms of the accretion rate in Eddington units, we find that, on average, the radius where the matter becomes thin to Thomson scattering could lie either inside or outside r_{ms} ; higher accretion rates lead to reflection edges at smaller radii.

The last of the four inner edges is the radiation edge, the smallest radius from which significant luminosity originates. This is difficult to locate on the basis of current simulations because they do not include either explicit dissipation or radiation. This edge is the most dependent on the detailed energetics of the accretion flow, both with respect to dissipation and photon escape. Estimates based on current work indicate that, like the reflection edge, it could lie on either side of r_{ms} , depending on circumstances. It is entirely possible that the disk can remain bright quite close to the black hole.

Although the simulations done so far are not ideally suited to determination of the inner edges relevant to observations, the dynamical features of the simulations should be more robust. One concern with the present simulations is that the accretion flow originates in an initial torus centered only $10r_g$ from the black hole. Although the dynamical disk edges occur well within the inflow region of the subsequent evolution, it is possible that specific details are influenced by the finite torus size.

The simulations done to date have also been restricted to relatively thick flows, with $h/r \approx 0.1$. The specific locations of the various edges depend only weakly on disk thickness. The turbulence edge likely moves inward slightly for smaller h/r . The location of the stress edge probably does not depend directly on h/r . Similarly, because surface density is independent of h , the location of the reflection edge depends more on factors such as the net accretion rate. Decreasing h tends to move the radiation edge inward, we expect, because, for fixed surface density, the diffusion time is $\propto h$. Future simulations should be able to refine these estimates.

In any case, while it is clear that any definition of a disk inner edge will lie in the vicinity of the marginally stable orbit, there is no reason why any of these inner edges should coincide *precisely* with r_{ms} . Depending on which physical concept is under consideration, any particular inner edge might be a factor of 2–3 inside or outside r_{ms} —and its position relative to r_{ms} can easily change as a function of time.

These facts have important implications with regard to the use of disk models as the basis for interpreting observations as probes of accretion in strong gravity. In virtually all previous efforts to interpret Fe $K\alpha$ profiles, the line shape was fit to a model that assumed the emissivity was a power-law in radius cut off abruptly at r_{ms} . However, as Reynolds & Begelman (1997) first pointed out, the reflection edge is not necessarily tied to the marginally stable orbit; as we have argued, it could as easily lie outside as inside that radius. Similarly, fits to the thermal portion of black hole accretion disk radiation are nearly always made with respect to models (such as the “multi-color disk”: Ebisawa et al. 1994, Shimura & Takahara 1995) that assume surface brightnesses following the Novikov-Thorne prescription or its Newtonian simplification. As we have shown here, this is unlikely to be a good description of the radiation edge. There is then little basis for the frequently-performed further step of using these model fits, in which the radiation edge is assumed to lie at exactly r_{ms} to infer a black hole’s mass and spin.

This work was supported by NASA grant NAG5-9187 to JHK, and NSF grant AST-0070979 and NASA grant NAG5-9266 to JFH. Computational support was provided by the San Diego Supercomputer Center of the National Partnership for Advanced Computational Infrastructure, funded by the NSF, and by the Legion project at the University of Virginia.

REFERENCES

- Abramowicz, M.A., Czerny, B., Lasota, J.P., & Szuszkiewicz, E. 1988, *ApJ*, 332, 646
- Abramowicz, M.A., & Kato, S. 1989, *ApJ*, 336, 304
- Agol, E., & Krolik, J.H. 1998, *ApJ*, 507, 304
- Agol, E., & Krolik, J.H. 2000, *ApJ*, 528, 161
- Balbus, S.A., & Hawley, J.F. 1991, *ApJ*, 376, 214
- Balbus, S.A., & Hawley, J.F. 1998, *Rev Mod Phys*, 70, 1
- Ebisawa, K., et al. 1994, *PASJ*, 46, 375
- Gammie, C.F. 1999, *ApJ*, 522, L57
- Hawley, J.F., Gammie, C. F., & Balbus, S.A. 1996, *ApJ*, 464, 690
- Hawley, J.F., & Krolik, J.H. 2001, *ApJ*, 548, 348 (HK01)
- Hawley, J.F., & Krolik, J.H. 2002, *ApJ*, 566, 164 (HK02)
- Krolik, J.H. 1999a, *ApJ*, 515, L73
- Krolik, J.H. 1999b, *Active Galactic Nuclei* (Princeton: Princeton Univ. Press)
- Lightman, A.P., & White, T.R. 1988, *ApJ*, 335, 57
- Miller, K., & Stone, J.M. 2000 *ApJ*, 534, 398
- Nandra, K., George, I.M., Mushotzky, R.F., Turner, T.J., & Yaqoob, T. 1997, *ApJ*, 477, 602
- Narayan, R., & Yi, I. 1995, *ApJ*, 444, 231
- Novikov, I.D., & Thorne, K.S. 1973, in *Black Holes*, eds. C. de Witt and B. de Witt (New York: Gordon & Breach), 343
- Page, D.N., & Thorne, K.S. 1974, *ApJ*, 191, 499
- Rees, M.J., Phinney, E.S., Begelman, M.C., & Blandford, R.D. 1982, *Nature*, 295, 17

Reynolds, C.S., & Armitage, P.J. 2001, *ApJ*, 561, L81

Reynolds, C.S., & Begelman, M.C. 1997, *ApJ*, 488, 109

Shimura, T., & Takahara, F. 1995, *ApJ*, 445, 780

Wilms, J., Reynolds, C.S., Begelman, M.C., Reeves, J., Molendi, S., Staubert, R., & Kendziorra, E. 2002, *MNRAS*, in press

Young, A.J., Ross, R.R., & Fabian, A.C. 1998, *MNRAS*, 300, 11